A Framework for Volt-VAR Optimization in Distribution Systems

Hamed Ahmadi, *Student Member, IEEE*, José R. Martí, *Fellow, IEEE*, and Hermann W. Dommel, *Life Fellow, IEEE*

***Abstract*—The possibility of leveraging the data provided by smart meters to understand the load characteristics is studied in this paper. The loads are modeled as voltage-dependent elements to increase the accuracy of volt-VAR optimization (VVO) techniques for distribution systems. VVO techniques are part of the distribution management system (DMS) and may be used for purposes such as loss reduction, voltage profile improvement, and conservation voltage reduction (CVR). A deterministic framework is proposed that formulates the VVO problem as a mixed-integer quadratically constrained programming (MIQCP) problem, which is solved efficiently using advanced branch-and-cut techniques. The proposed framework is capable of optimally controlling capacitor banks, voltage regulators, and ULTCs for day-ahead operation planning. The results indicate that loss reductions of up to 40% and a total demand reduction of up to 4.8% are achievable under some loading conditions in a radial test system. The effect of the load voltage dependence is also demonstrated through analytical simulations.**

***Index Terms*—Distribution systems, volt-VAR optimization, mixed-integer programming.**

I. Introduction

DISTRIBUTION systems (DS) have been conventionally operated with minimal automation. Simplicity of system operation has received a higher priority than its optimality. A typical DS has distinct features that make it different from a typical transmission system, such as relatively high R/X ratio, radial configuration, limited automation and minimal visibility of the system condition. For instance, there is no information about the voltage quality at the end of the feeders.

In the past couple of decades, a rapid movement towards DS automation has been started by many power utilities worldwide to increase efficiency, reliability, resiliency, and power quality. As the heart of DS automation, distribution system management (DMS) tools are being introduced as counterparts to the energy management system (EMS) tools that exist for the optimal operation of transmission systems. The DMS concept offers many appealing functionalities, including state estimation, fault location, service restoration, and volt-VAR optimization (VVO). The VVO functionality, which is the main target of this study, is basically defined as the optimal control of the system equipment (e.g., capacitor banks, voltage regulators, ULTCs, etc.) in order to satisfy objectives such as minimizing the losses, improving voltage profile, etc.

Many utilities have already deployed a number of VVO applications and promising results are being reported. Good examples are the Northern State Power Company [1], B.C. Hydro [2]-[4], Taiwan Power Company [5], and American Electric Power [6]. Besides loss reduction and voltage profile improvement, VVO offers one more useful capability: the so-called conservation voltage reduction (CVR). The CVR essentially refers to reducing the voltage magnitudes to the minimum allowable in order to reduce the demand, especially for peak shaving purposes. It stems from the fact that loads are voltage-dependent with a positive slope, i.e. reducing the voltage yields a reduction in both active and reactive demands. An immediate reaction to this concept would be a concern towards the voltage quality at the customer terminals. The deployment of the advanced metering infrastructure (AMI) has provided enormous visibility for almost all the nodes in the DS, facilitating the application of CVR with a high confidence in the quality of power delivery [4]. Practical studies have shown that, upon proper implementation of CVR, a demand reduction of 1% to 6% in the total demand can be achieved [4].

Several VVO methodologies have been proposed in the literature. An algorithm based on the oriented discrete coordinate descent method is proposed in [7], which gives priority to finding a feasible but suboptimal solution in a short time rather than finding the global optimum, which may impose a high computational burden. A supervisory control scheme was developed in [8] that takes advantage of the measurements available at the substation to optimally adjust the voltage regulators and capacitor banks at the substation as well as over the feeders. The VVO problem is decomposed into two subproblems, at substation and feeder levels, in [9], which are then solved using a simplified dynamic programming and a fuzzy logic control algorithm. In [10], the VVO problem is solved using an adaptive neuro-fuzzy inference system. A multiobjective Genetic Algorithm, improved by fuzzy logic, is applied to the VVO problem in [11], in which the size of the combinatorial search space is reduced using expert knowledge.

A Genetic Algorithm method is proposed in [12] for CVR using capacitor placement. While there are limited academic publications on the subject of CVR methodologies, the industry is progressing gradually in implementing CVR, mostly for peak-shaving. The key factor that governs the efficiency of VVO and CVR implementations is the voltage dependence of loads, as is acknowledged in [13]. Preliminary tests at BC Hydro have shown a strong dependency of the active and reactive power demands on the voltage magnitude [2], which encourages the concept of voltage reduction to save energy. However, some loads may need to stay ON for a

This work was supported by the National Science and Engineering Research Council (NSERC) of Canada. The authors are with the Department of Electrical and Computer Engineering, University of British Columbia, Vancouver, BC, V6T 1Z4, Canada (e-mail: hameda@ece.ubc.ca; jrms@ece.ubc.ca; hermannd@ece.ubc.ca).

longer period of time to carry out the same task, compared to a normal voltage level. These loads are usually equipped with a thermostat, e.g., air conditioners, space heaters, etc. Although these loads may stay ON for longer period as a result of CVR, the total consumed power can be reduced at the peak and shifted to the next period of time after the peak. The estimation of the loads' voltage dependence has a significant impact on the performance of the VVO algorithms.

At the distribution system level, the deployment of smart meters has provided enormous amount of data on load behavior. Since the basic functionality of most of the commercial smart meters involves capturing the waveforms of current and voltage, and conducting calculations based on those waveforms, there is a significant opportunity to leverage the available waveforms to recognize the load. Many algorithms have been proposed for load disaggregation at the smart meter level, e.g. [14]. Once these algorithms are implemented, the type of connected appliances at each customer terminal is available at any time instant. Knowing the type of load, one can estimate the voltage dependence of the aggregated load at each distribution transformer level. In an extensive study conducted by the Electric Power Research Institute (EPRI), the voltage dependence characteristics of major appliances are derived based on laboratory measurements [15]. Having both the load types and the voltage dependence of each type, an accurate-enough estimation of the aggregated load voltage dependence can be performed.

In this paper, a framework for implementing VVO in modern distribution systems is proposed. This framework takes into account the voltage dependence of loads, utilizes the linear power flow (LPF) formulation of [16], and formulates the operation planning problem as a mixed-integer quadratically constrained programming (MIQCP) problem that can be solved efficiently to its global optimum. The analysis is truncated at the distribution transformer level, which is the primary network, and the secondary network is modeled as an aggregated load with a known composition. Capacitor banks, voltage regulators, and under-load tap changing (ULTC) transformers are considered as the control variables and the problem is formulated for a day-ahead period.

The rest of the paper is organized as follows. In Section II, the load modeling procedure is described. The VVO algorithm is explained in Section III. Simulation results are provided in Section IV. The concluding remarks are given in Section V.

II. Voltage-Dependent Load Modeling

Traditionally, loads are roughly categorized as residential, commercial, and industrial [17]. For each load type, some typical characteristics are then derived based on historical measurements. For today's distribution system, however, this level of decomposition is not sufficient. The smart meters installed at the customer level are capable of capturing load variations and even recognizing the load types. The load composition at each meter can then be aggregated at the distribution transformer level to create an estimate of the total load composition at the secondary network fed by each distribution transformer. Without loss of generality, a residential area is considered in this study. The number and types of on-line appliances vary during a 24-hour period. The pattern for weekdays are quite similar, while the weekends have different patterns than the weekdays. The load composition also changes according to weather conditions, season, geographical location, etc. This implies the need for load modeling and estimation schemes for every single feeder during a period of time to be able to create a relatively accurate load model and forecast.

The voltage-dependent load models generally used in power system studies are the ZIP model, the exponential model, and other higher-order polynomial models. The idea behind all of these models is to fit a curve to the measured data to represent the voltage dependence of active and reactive power demand. This fact has been utilized by the authors in [16] to, first, assume a voltage-dependent load model and, second, formulate the power flow as a linear problem. The load model used in [16] can be described as:

$$\frac{P(V)}{P_0} = C_Z \left(\frac{V}{V_0}\right)^2 + C_I \left(\frac{V}{V_0}\right) \tag{1}$$

$$\frac{Q(V)}{Q_0} = C'_Z \left(\frac{V}{V_0}\right)^2 + C'_I \left(\frac{V}{V_0}\right) \tag{2}$$

in which P and Q are the load's active and reactive power consumption; V is the terminal voltage magnitude and the zero subscript indicates the nominal value; constants C and C' are calculated by an ordinary least squares (OLS) curve-fitting procedure. Note that $C_Z + C_I = 1$ and $C'_Z + C'_I = 1$. As it is shown in [16], this synthesis is accurate-enough to model the load characteristics within the normal operation voltage range.

There are many different appliances in a typical residential home. Nonetheless, for the purpose of load modeling for applications such as VVO, some appliances may be ignored due to their minor impact on the total demand response. For instance, a phone charger, which is typically rated at 5 W, does not influence the demand response of a house with, say a 2 kW total demand. This fact also relieves the accuracy requirement on the disaggregation scheme implemented at smart meters. In addition, there are appliances with relatively high power demand which are only used for a very short period of time. For instance, a microwave oven, which may be rated at 1.5 kW to 3 kW, is typically used for only a few minutes to warm up foods. These types of load are also of no importance for the VVO application, assuming an action time window of, say, 30 minutes. Taking into account the mentioned points, the number of appliances that need to be detected and properly modeled is reduced to a manageable extent. A list of typical major appliances for a residential customer are given in Table I along with a load tag to be used later in this paper. Note that this list is generated according to a typical cold-climate household and it may vary for different countries and/or climates.

Residential customers can be further divided into two categories: 1) with residents leaving the place for work during the day, and coming back during the afternoon/evening (House 1); 2) with residents staying at home most of the time (House 2). Besides, around the residential areas, it is very common to find small businesses such as restaurants and convenience

Table I
LIST OF TYPICAL APPLIANCES FOR A RESIDENTIAL AREA

Type	Water Heater	Space Heater	Refrigerator
Tag	No. 1	No. 2	No. 3
Type	Electronics	Incand. Light	Fluor. Light
Tag	No. 4	No. 5	No. 6
Type	Dishwasher	Washing Machine	Clothes Dryer
Tag	No. 7	No. 8	No. 9
Type	Electric Range	Vacuum Cleaner	Ventilation-Fan
Tag	No. 10	No. 11	No. 12
Type	Induction Cooker	HP Sodium Light	Air Conditioner
Tag	No. 13	No. 14	No. 15

stores. Also, street lights are connected to a designated distribution transformer on the same feeder. This information is obtained by studying a typical residential area in Vancouver, BC, Canada, and sample data is generated for the purpose of simulation. For the four types of customers mentioned earlier: House 1, House 2, Restaurant, and Street Light, a typical load composition over a 24-hour period during a weekday is shown in Figs. 1(a)-1(d). A combination of these loads may be connected to a distribution transformer. For thermostatic loads, e.g. refrigerators, the ON/OFF time intervals vary from customer to customer so that, at an aggregated level, there are always a few refrigerators on-line. In a more sophisticated version of this framework, every appliance may be from different manufacturer, and may exhibit different voltage dependence characteristics. For instance, the fluorescent lamps may be driven by an electronic or magnetic ballast [18], which may exhibit different voltage-power characteristics. In this paper, a simplified version of load types is assumed for illustration purposes. The voltage dependence of a variety of appliances were derived in [15] using extensive laboratory measurements. For the sake of completeness, a sample of the data is reproduced here for some typical devices. Figure 2 depicts the per-unit values of active and reactive power consumptions of the devices for a range of 0.9 p.u. to 1.05 p.u. of the terminal voltage. Once the total demand for each type of device at a distribution transformer is known, the corresponding graph in Fig. 2 is multiplied by those values and a voltage-dependent model for that load is generated. This is done for all other types of devices and the sum of all the scaled graphs will provide the voltage dependence characteristic of the total load connected at a particular distribution transformer at a specific time. The core losses of distribution transformers are also modeled here as a voltage-dependent load in parallel with the load connected to that transformer. The voltage dependence of the core losses of a typical distribution transformer is shown in Fig. 3 [15]. The winding losses as well as the secondary network impedance can also be considered in series with the corresponding lump load. A Norton equivalent of this impedance and the load is then derived to represent the augmented load model. It is trivial to calculate the parameters in (1) and (2) based on the generated data for the lump load [16].

The outcome of the above analysis is to have an estimation of the parameters in (1) and (2) for each node in the system

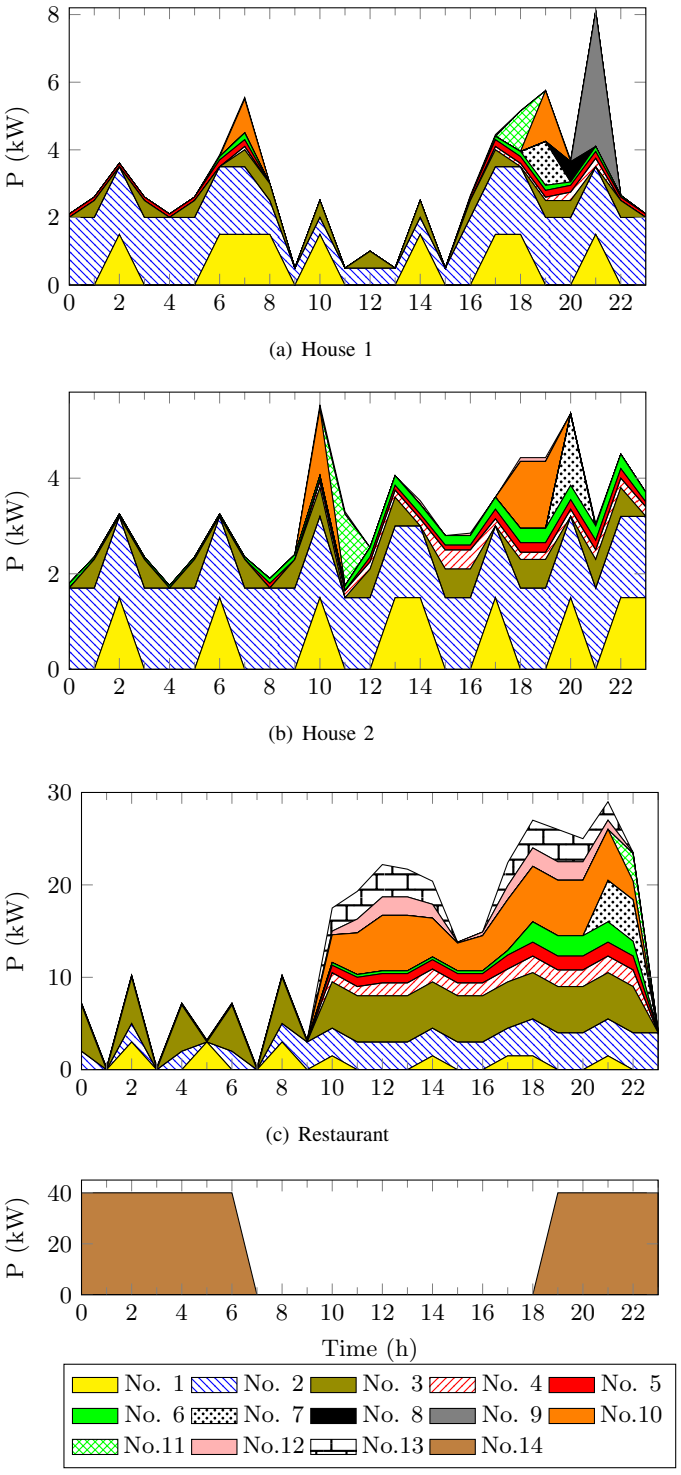

(a) House 1

(b) House 2

(c) Restaurant

(d) Street Light (100×HP Sodium light)

Figure 1. Typical load profile for a residential area in a weekday.

to be incorporated in the power flow analysis.

III. VOLT-VAR OPTIMIZATION ALGORITHM

The problem of distribution system volt-VAR optimization (VVO) is, in some ways, similar to the unit commitment problem in the transmission system. In the unit commitment problem, the status of each unit is to be determined during

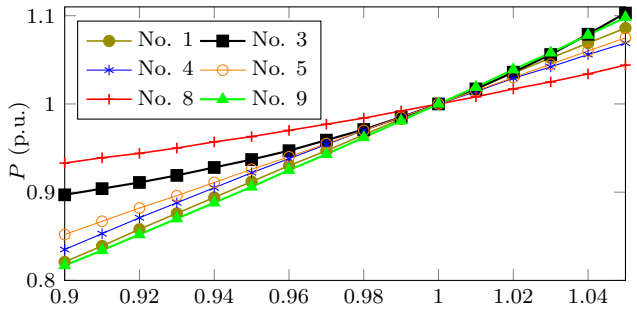

(a) Active Power

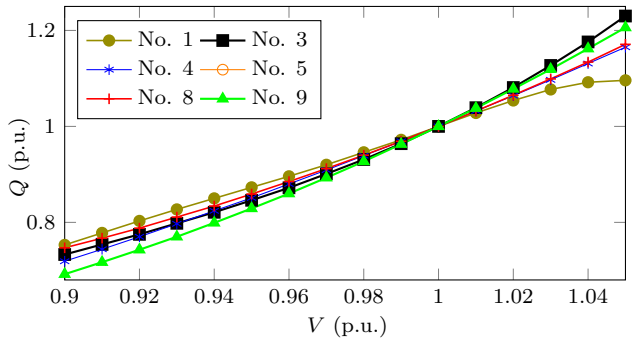

(b) Reactive Power

Figure 2. Voltage dependence characteristics of typical appliances [15].

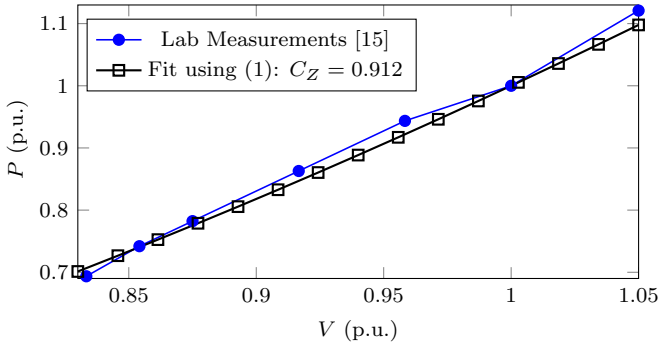

Figure 3. Distribution transformer core losses voltage dependence [15]. Ratings: 50 kVA, 12.47kV/120V, nominal core losses = 124W.

a certain period of time, say for a day-ahead, to minimize the total generation cost. Similarly, in the VVO problem, the statuses of capacitor banks, voltage regulators, and ULTC's are to be determined for a day-ahead period, assuming a forecast for the demand, in order to satisfy objectives such as minimizing network losses. This is particularly important because of the fact that the number of switching actions has to be limited. Switch operations will reduce the lifetime of the equipment. Therefore, the problem cannot be decoupled for each time interval, i.e. the solution at the current time step is dependent on the previous and next time steps. This characteristic requires the problem to be formulated for the whole period of the planning horizon which, in turn, drastically increases the problem dimensionality. To cope with this problem, simplifications are sought in this paper to reduce the dimensionality while respecting a certain level of accuracy.

Once the status of all system equipment are determined, minor adjustments can be made in near-real-time to compensate for possible errors in the predictions and/or to respond to a contingency. This mimics very well the concept of optimal power flow for real-time adjustments, based on the unit commitment schedule. For instance, equipment with continuous adjustment capabilities such as distributed generators, distributed energy storages, distribution static compensators, and interruptible loads are perfect candidates for near-real-time adjustments, especially for reactive power support. In addition, the status of the mentioned equipment does not need to be determined ahead of time since these are almost always connected to the gird. In this study, the problem of day-ahead scheduling of switchable equipment is studied and the problem of near-real-time adjustments is left as future work of the research group.

A. The Linear Power Flow Formulation

Distribution systems (DS) are known for the unbalance of the phase currents, which stems from the non-uniform distribution of single-phase loads at the household level. To run an accurate load flow, a three-phase algorithm is required. However, for some specific applications, it may be accurate-enough to model the single-phase loads as balanced three-phase loads. Most of the capacitor banks, voltage regulators, and ULTCs are three-phase units, i.e. a switching action involves all three phases simultaneously. In addition, all the analysis done in this paper deals with the primary distribution network, which includes the LV network between the substation and the secondary distribution transformers. These characteristics make it a valid approximation to model primary distribution system as a balanced network.

A linear power flow (LPF) formulation is derived in [16] which takes into account the voltage dependence of loads and assumes small voltage angles. Using the load model described by (1) and (2), each load can be represented by its Norton equivalent, which is basically a current source in parallel with an admittance. Applying the nodal analysis to the resulting network, the LPF equations can be derived, as discussed in [16]. In Cartesian coordinates, the LPF is expressed as:

$$\sum_{k=1}^{n} \left(\bar{G}_{m,k} V_k^{\text{re}} - \bar{B}_{m,k} V_k^{\text{im}} \right) = I_{p,m} \tag{3}$$

$$\sum_{k=1}^{n} \left(\bar{G}_{m,k} V_k^{\text{im}} + \bar{B}_{m,k} V_k^{\text{re}} \right) = I_{q,m} \tag{4}$$

where $\bar{G}$ and $\bar{B}$ are the real and imaginary parts of the admittance matrix; n is the number of nodes; m and k are the nodes at the two ends of the branch connecting Node m to Node k; V^{re} and V^{im} are the real and imaginary parts of the nodal voltages, respectively. Note that the impedance parts of the loads are added to the corresponding diagonal elements of $\bar{G}$ and $\bar{B}$ and the current injection parts appear in the right-hand side of (3) and (4) as I_p and I_q.

A capacitor bank is modeled here as an admittance element $\bar{B}^c$, which then appears in the corresponding diagonal

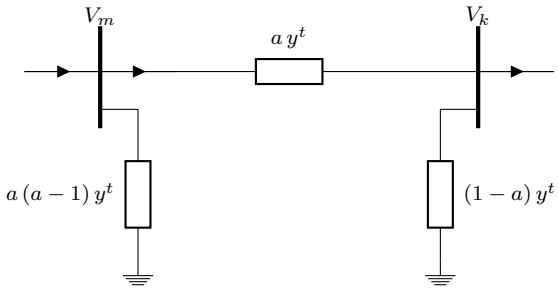

Figure 4. The π-equivalent circuit of a ULTC-equipped transformer.

elements of $\bar{B}$, i.e.:

$$B_i^c = u_i\,\bar{B}_i^c \tag{5}$$

Here $u_i \in \{0,1\}$ represents the status of the capacitor bank connected at Node i.

A transformer with under-load tap changing (ULTC) capability is modeled using the π-equivalent circuit [19], as shown in Fig. 4. In this figure, a stands for the transformer ratio and y^t is the transformer admittance for $a = 1$. The two shunts on both sides compensate for the different tap ratios to model the voltage buck/boost. For the sake of simplicity, the transformer impedance is assumed to be inductive. In order to linearize the term $a\,(a-1)$ for $0.9 \le a \le 1.1$, it is approximated by $a - 0.9963$ which places a maximum error of 0.08% in the voltage magnitudes in the simulated systems. It should be noted that a is a discrete variable and can only take values between 0.9 and 1.1 with steps of, e.g., 0.01, which yields 20 steps in total. This leads to the following mathematical representation:

$$a = \sum_{j=1}^{20} b_j x_j \;,\quad \sum_{j=1}^{20} x_j = 1 \tag{6}$$

in which $x_j \in \{0,1\}$ and $b_j \in \{0.9, 0.91, \ldots, 1.1\}$. The last equality constraint in (6) is a special ordered set (SOS) which can be efficiently handled by commercial mixed-integer programming solvers.

A multiplication of binary-continuous variables may be encountered by adding (5) or (6) to the modified admittance matrix elements in (3) and (4). Assume z is a binary variable and r is a continuous variable bounded by $r^{\min} \le r \le r^{\max}$. The multiplication of these variables, i.e. $w = z\,r$, can be linearized by adding the following constraints to the problem:

$$r - (1-z)\,r^{\max} \le w \le r - (1-z)\,r^{\min} \tag{7a}$$

$$z\,r^{\min} \le w \le z\,r^{\max} \tag{7b}$$

If $z = 1$, (7a) forces w to be equal to r and (7b) ensures that r falls within its bounds. If $z = 0$, (7b) forces w to be zero and (7a) is an inactive constraint since r always falls within its predefined bounds. Therefore, w can replace $z\,r$, providing that (7a) and (7b) are added to the problem as constraints.

The VVO problem may have different objectives, such as loss reduction, voltage profile improvement, and conservation voltage reduction (CVR). These objectives as well as the corresponding system operational constraints are described in the following subsections.

B. Active Loss Reduction

The active power losses are calculated as:

$$P_{\text{loss}} = \sum_{m<k} \bar{G}_{m,k}\left[(V_m^{\text{re}} - V_k^{\text{re}})^2 + (V_m^{\text{im}} - V_k^{\text{im}})^2\right] \tag{8}$$

which is a convex quadratic term for fixed values of $\bar{G}$. It should be noted that the binary variables associated with the ULTC's only appear in $\bar{B}$ and, hence, have no effect on (8).

C. Conservation Voltage Reduction

The CVR technique is usually used to reduce the total power drawn from the substation or a particular feeder in order to meet the thermal limits of the equipments, peak load shifting (or shaving), and reducing carbon dioxide emissions by lowering power generation. Since the voltage magnitude at the substation is considered to be a given quantity, the outgoing power from the substation can be defined by the summation of all the currents through the outgoing feeders. According to (3) and (4), and considering the direction of the current injections, the active and reactive power drawn from the substation can be calculated as:

$$P_s = -V_s \sum_{k=1}^{n} \left(\bar{G}_{s,k} V_k^{\text{re}} - \bar{B}_{s,k} V_k^{\text{im}}\right) \tag{9}$$

$$Q_s = V_s \sum_{k=1}^{n} \left(\bar{G}_{s,k} V_k^{\text{im}} + \bar{B}_{s,k} V_k^{\text{re}}\right) \tag{10}$$

in which the subscript s represents the quantities related to the substation. Depending on the requirements of the system operation, P_s, Q_s, or a combination of them, may be minimized in the context of CVR. Note that minimizing the power drawn from the substation may implicitly increase the losses since lowering the voltages in order to reduce the demand sometimes increases the losses. However, the amount of reduced demand is sufficiently larger than the losses so that the increase in losses does not become an issue.

D. System Operational Constraints

According to the grid code requirements, there are certain limits that must be respected during normal operation conditions. The basic grid code constraints are the nodal voltage limits and the branch ampacities. Since the voltage angles are quite small, the nodal voltage limits can be expressed as:

$$V^{\min} \le V_i^{\text{re}} \le V^{\max} \tag{11}$$

The magnitude of the current flowing through Branch m-k is calculated as:

$$I_{m,k}^2 = [\bar{G}_{m,k}^2 + \bar{B}_{m,k}^2][(V_m^{\text{re}} - V_k^{\text{re}})^2 + (V_m^{\text{im}} - V_k^{\text{im}})^2] \tag{12}$$

The branch ampacity limits can be written as follows:

$$I_{m,k}^2 \le I_{\max}^2 \tag{13}$$

which is a convex quadratic constraint.

The number of switching operations on each switchable equipment (with mechanical switches) needs to be limited to avoid reducing the lifetime of that equipment. On the other hand, an equipment that is controlled through power electronic switches does not have this limitation. Since operation planning covers a period of time, say T, with fixed time steps, say h, a switching action can be defined as the change in the status of a switch for two consecutive steps. Mathematically, it can be expressed as:

$$\delta_{i,t} = |u_{i,t} - u_{i,t-h}| \tag{14}$$

in which $\delta_{i,t} = 1$ if a change occurs in the status of unit i from $t-h$ to t, and $\delta_{i,t} = 0$ otherwise. Since most of the optimization routines cannot handle the absolute value operator, the following variant of (14) is used instead:

$$\delta_{i,t} = (u_{i,t} - u_{i,t-h})^2 \tag{15}$$

which admits the same value of (14) as long as u is a binary variable. The total number of switching actions for an equipment over the planning horizon can then be calculated as:

$$\alpha_i = \sum_{t=h}^{T} \delta_{i,t} \tag{16}$$

As discussed earlier, the number of total switching actions for an equipment needs to be limited. There are two ways for doing this. The first way is to add (16) to the objective function with some appropriate weight and solve for a multi-objective function. In order to choose a proper weight, the monetary value of each switching action is needed as well as the monetary value of the other objective, e.g., losses. This data is difficult to obtain and the authors have no access to such information. The second way is to add a limit based on experience. This can be formulated as a simple constraint:

$$\alpha_i \leq \alpha_i^{\max} \tag{17}$$

Without loss of generality, the second method is adopted here.

IV. Simulation Results

A. Test System Description

The 69-Node distribution system of [20] is used here to demonstrate the proposed framework. Some modifications are applied to this system. The system power flow data are reproduced in Table II to indicate the modifications. The load data in Table II is considered as the peak demand during the day, with the load curve shown in Fig. 5 for the entire day. The total load at peak is $5.3 + i\,3.8$ MVA. In order to apply control strategies, four capacitor banks rated at 750 kVAR are installed at Nodes 15, 25, 53, and 62, as shown in Fig. 15. A voltage regulator is assumed between Nodes 6 and 7, as shown in Fig. 15, with an impedance of $0.0801 + i\,1.6028\ \Omega$, equipped with 20×0.01 taps providing a discrete voltage range of 0.9 to 1.1 p.u. The core losses in the distribution transformers are a function of the primary network voltage, as described in Fig. 3. These core losses are added to each node as a voltage-dependent load. The transformer winding losses are modeled as a series resistance with load. A simple circuit analysis yields the Norton equivalent of the distribution transformer and the load connected to it. Nodes 21, 31, 41, and 60 are assumed to be the street lights suppliers for the corresponding block(s), with HP Sodium lights as their load. For other nodes, random combinations of House 1, House 2, and Restaurant are assumed, as explained in Section II. The nodal loads are then aggregated at the substation to form the load curve shown in Fig. 5.

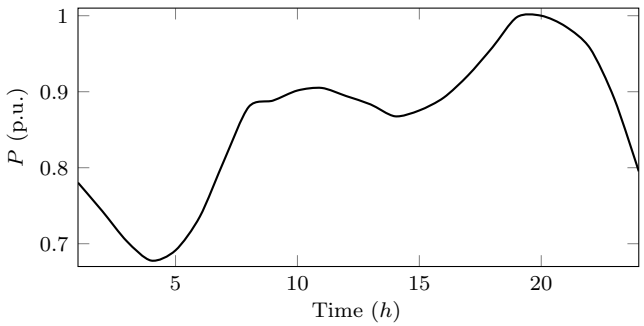

Figure 5. Daily load curve for the 69-Node feeder.

All the simulations are done in the GAMS platform and CPLEX is used to solve the mixed-integer quadratically constrained programming (MIQCP) problem formulated in Section III. The solver uses a branch-and-cut algorithm to efficiently solve the MIQCP problem [21]. The following abbreviations are used in all the figures:

- Original: All capacitors are "OFF" and $a = 1$.
- No Control: All capacitors are "ON" and $a = 1.01$.
- R-LR: Loss reduction in radial network.
- R-CVR: CVR in radial network.
- L-LR: Loss reduction in looped network (Switch 50-59 is closed).
- L-CVR: CVR in looped network (Switch 50-59 is closed).

B. Loss Reduction

In this objective, the VVO routine is set to minimize the active power losses, as described in Section III. In order to show the impacts of the capacitors and the voltage regulator on the total power consumption and the losses, a continuous range of variation for the tap position (from 0.9 to 1.1) and the capacitor sizes (from 0 to 1 MVAR) is considered. All capacitors are assumed to take the same size at this part. The total losses are shown in Fig. 6 for the radial network. It can be clearly seen in Fig. 6 that there is an optimal value for both the capacitor sizes and the tap ratio that minimizes the total losses for the peak load condition. The actual problem, however, is not as simple as this. Each segment of load curve during the day and the maximum allowable switching operations that chain those segments complicate the problem substantially.

Similar to what is shown in Fig. 6 for the active power losses, the total power drawn from the substation varies as the tap position and capacitor size increase. A relatively linear pattern is observed in the total demand versus tap position, which can roughly be stated as follows: a 1% increase in

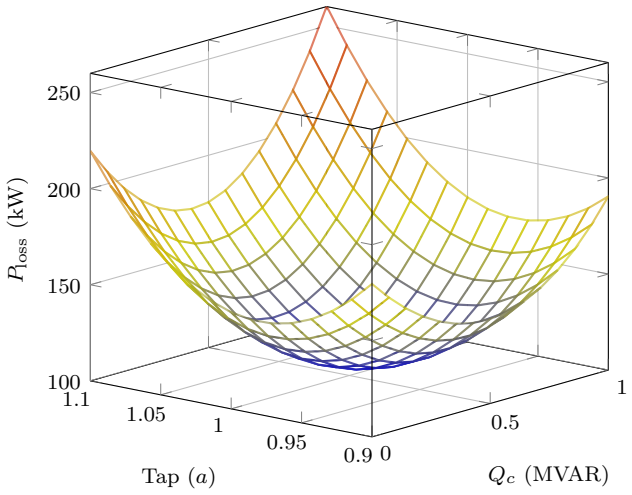

Figure 6. Total power losses at peak load.

tap ratio (a) leads to a 1.5% increase in the active power demand (P_s) and 2.2% in reactive power demand (Q_s). For the capacitor sizes (Q_c), on the other hand, a more interesting behavior was observed. P_s turned out to be a quadratic function of Q_c: $P_s = 195.1\,Q_c^2 - 64.8\,Q_c + 4916$, where P_s is in kW and Q_c is in MVAR. This shows that for up to 166 kVAR of capacitors, the total demand will decrease and if Q_c is increased beyond this value P_s will increase quadratically. Comparing this with the results in Fig. 6, it shows that when Q_c increases from 0 to 166 kVAR, the reduction in the losses dominates the increase in the demand. Beyond this value, however, the situation reverses. It is worthwhile mentioning that, as seen in Fig. 6, the minimum loss occurs at $Q_c \approx 460$ kVAR.

The total reactive power demand (Q_s) decreases, although slowly, as the size of capacitors increases (0.5% reduction in Q_s for a 1% increase in Q_c). There are two factors contributing to this behavior. The improvement in the voltage profile due to the installed capacitors will increase the reactive power demand, while the total reactive power drawn from the substation is reduced due to the local reactive power supply provided by the capacitors. These two factors work against each other and, thus, compromise the effect of Q_c on Q_s.

The above discussion reveals the sensitivities of P_s, Q_s, and P_{loss} to the control variables. In this part, a case is analyzed over a 24-hour period with time spans of 2 hours, i.e. 12 steps in total. The amount of load and its characteristics at each node is updated every two hours and the status of the capacitor banks (750 kVAR each) and the tap position (a) are determined using the VVO algorithm to minimize the losses. A $\pm 6\%$ deviation from the nominal value is allowed for nodal voltages.

For loss reduction in the radial network, the optimum tap and capacitor settings are given in Fig. 7. The total active power demand P_s and the active power losses are shown in Figs. 8 and 10, respectively. The minimum nodal voltage is shown in Fig. 11. By installing capacitors and the voltage regulator in the original network, the reactive power demand from the substation Q_S is substantially reduced in "No Control" case, as shown in Fig. 9. Performing the LR strategy, however, increases the reactive power drawn from the substation. This is due to the fact that Q_S is not part of the problem formulation. The reactive power demand at the substation can be compensated by substation capacitors or other shunt compensators. Also, one may need to solve a multi-objective problem or limit the amount of Q_S to the reactive power capability of the substation, should that become a concern. In order to see the amount of reductions achieved in this case, refer to Fig. 12 for P_s and Fig. 13 for P_{loss}. It is interesting to see that over 40% reduction in losses can be achieved at midnight, whereas about 20% reduction is possible around the peak load. This alone shows the inefficiency of a fixed setting for control devices due to a large variation in load during the day.

Topology of the network plays a crucial role in system operation. For instance, by closing Switch 50-59 and creating a loop in the 69-node system, the total losses are reduced by 36% in the original case at peak load. This fact is also reflected in Fig. 13 with higher values of achieved loss reductions. Loss reduction also flattens the voltage profile throughout the network, as shown in Fig. 11. The new optimum settings obtained for this case are shown in Figs. 14(a) and 14(b).

C. Conservation Voltage Reduction

The intentional reduction in nodal voltages across the network to achieve a reduction in the total demand is referred to as conservation voltage reduction (CVR). The critical criteria in practicing CVR is to ensure that all the nodal voltages fall within the acceptable standard range. Assuming a minimum allowable voltage of 0.94 p.u. and setting the objective at minimizing P_s in (9), the optimization problem is solved for a day-ahead operation. The aim here is to see the effect of CVR at different hours during a typical weekday. The results for P_s and P_{loss} under the CVR is shown in Figs. 8 and 10. The optimal settings for the capacitor banks and tap ratio under CVR are given in Fig. 7. The reductions yield by applying the CVR technique are shown in Figs. 12 and 13. It is interesting to see that the CVR is more effective during light load condition (1 AM to 5 AM) when up to 4.8% reduction in the total demand is achieved. This occurs due to the fact that light load leads to higher voltages which, in turn, translates into an unnecessary increase in demand. Another contributing factor is the inefficiency of a fixed setting for capacitor banks and voltage regular for the entire day. These devices are normally designed to mitigate the system operation requirements at the peak load, which is obviously not efficient for other periods. Optimally adjusting the volt-VAR controllers in the system, the demand can be deliberately reduced. At the peak load, on the other hand, the voltages are pushed down to the lower bound and, therefore, there is less room for further decreasing the voltage for demand reduction.

The effect of having a weakly-meshed network on CVR factor is studied here. A loop is formed by closing Switch 50-59. The new results for this case are shown is Fig. 8, labeled as L-CVR. As can be seen, the effectiveness of CVR

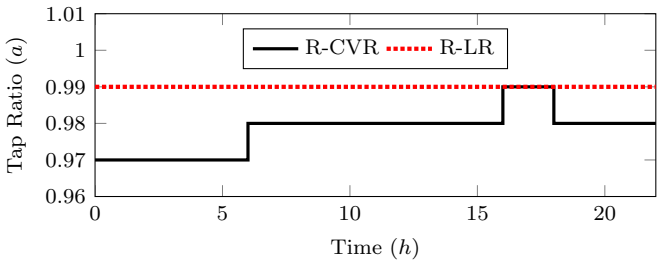

(a) Tap ratio (a)

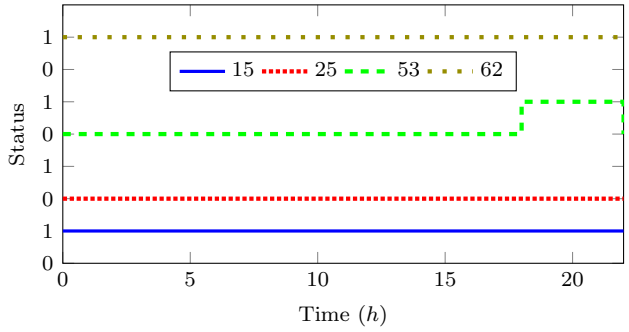

(b) Capacitor banks statuses under R-LR

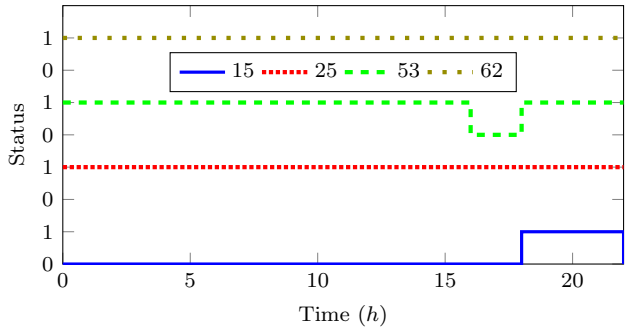

(c) Capacitor banks statuses under R-CVR

Figure 7. Tap ratio and capacitor banks statuses under different objectives for the radial network.

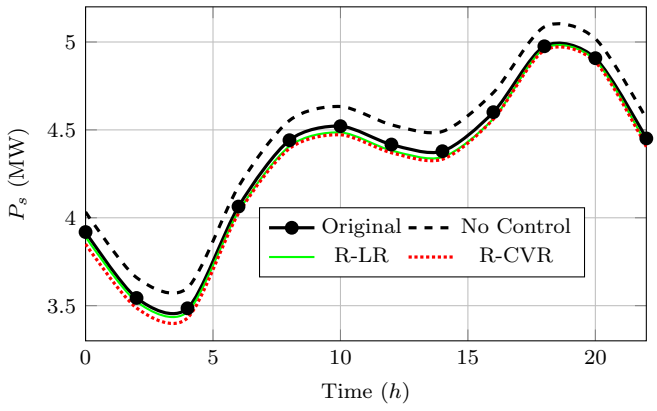

Figure 8. Total active power drawn from the substation.

on demand reduction is reduced in the looped network. This occurs due to the fact that closing a loop has two important effects on the network. The first effect is to improve the

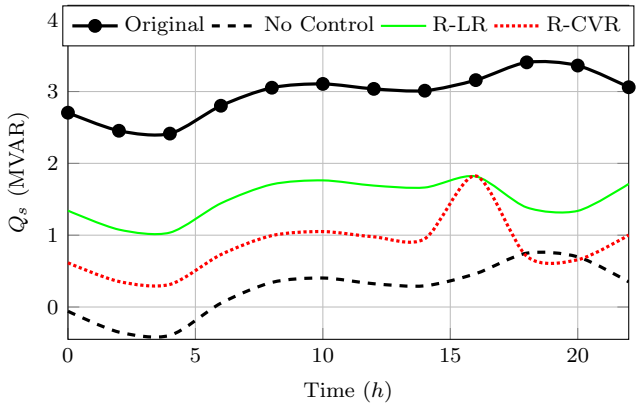

Figure 9. Total reactive power drawn from the substation.

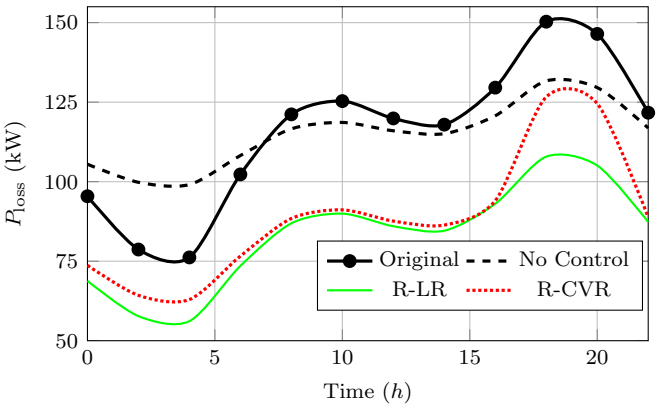

Figure 10. Total active power losses.

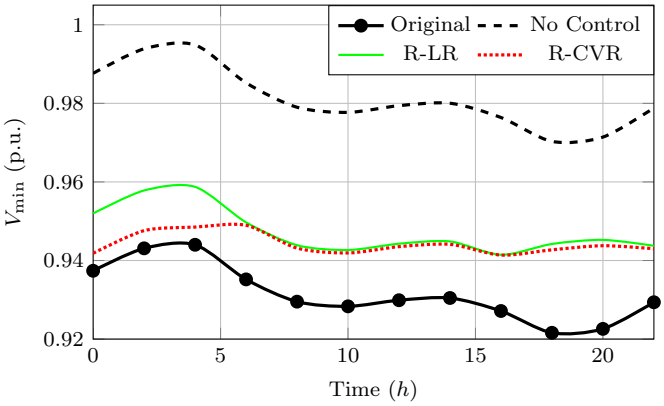

Figure 11. Minimum nodal voltage.

voltage profile in the original case. Having a good voltage profile without any extra reactive power support limits the maneuvering capabilities in controlling the voltage profile and deliberate voltage reduction. The second effect is to create dependencies between nodal voltages, i.e. increasing the voltage at the beginning of the feeder (e.g., Node 50) would also increase it at nodes connected to the end of the feeder (e.g., 59) and vice versa. These two factors have considerably reduced the CVR factor. The new optimum settings for this case are given in Figs. 14(a) and 14(c).

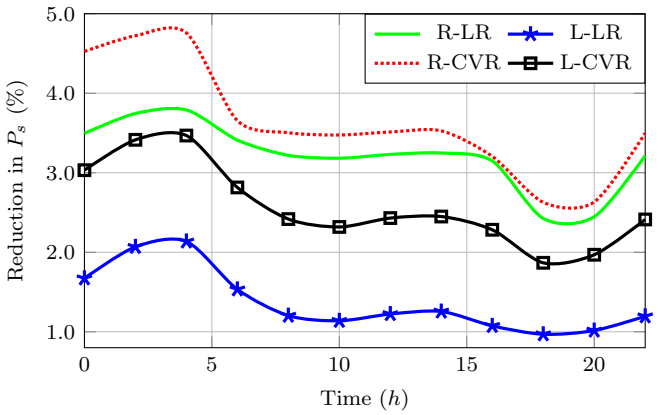

Figure 12. Reduction in total active power demand w.r.t. "No Control" case.

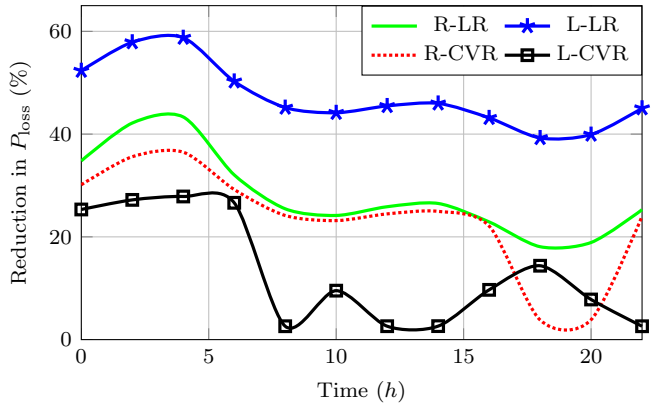

Figure 13. Reduction in total active power losses w.r.t. "No Control" case.

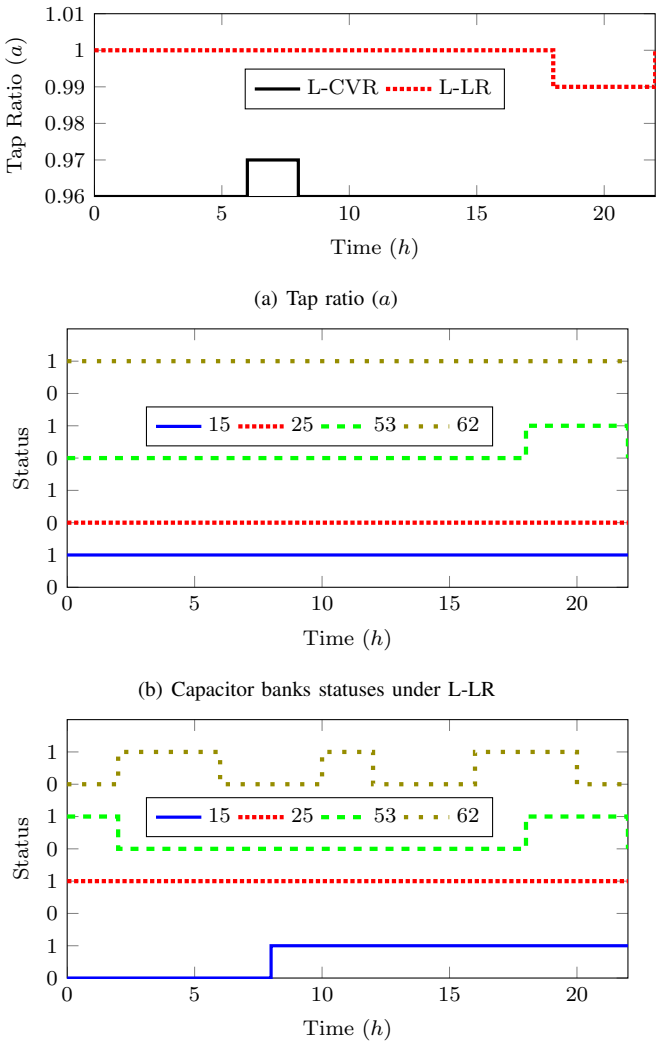

(a) Tap ratio (a)

(b) Capacitor banks statuses under L-LR

(c) Capacitor banks statuses under L-CVR

Figure 14. Tap ratio and capacitor banks statuses under different objectives for looped network (Switch 50-59 is closed).

Comparing the CVR and LR outcomes, it can be concluded that at light loads CVR yields greater reductions in total demand, whereas LR yields greater reductions in total losses at the peak load. At other hours, the two objectives produce similar reductions in both total demand and power losses. As shown in Fig. 9, the reactive power drawn from the substation is higher in the LR case. It should be noted that CVR may not be activated during the entire day but for peak shaving/shifting purposes. In order to accurately calculate the amount of shifted demand from the peak hour to the next adjacent hour, the thermostatic loads have to be modeled as time-dependent elements in addition to their voltage dependence. This means that part of the reduced demand may come back during the next hour adding up to the expected load forecast. In order to model these characteristics, a more through understanding of load behavior is required.

V. Conclusion

A framework for formulating and implementing volt-VAR optimization (VVO) techniques is proposed. Loads are modeled as voltage-dependent elements and the variation of load characteristics during the day is taken into account. Smart meters are taken advantage of to establish a platform for load disaggregation, thus providing good estimates of the loads' voltage dependence characteristics for every node and at every time interval. The results in this paper indicate that by optimally controlling the voltage and VAR devices in a distribution system, some reductions in both losses and total demand may be achieved. It is also concluded that CVR techniques are more effective at light load conditions, where there is more room for pushing the voltages down to their limits. A fairly large reduction in total power losses (ranging from 20% to 40%) is also achievable by applying a proper control scheme, as compared to a conservative fixed setting for peak load conditions. Should the operator seek to activate the CVR for the entire day, a more comprehensive model of the thermostatic loads must be developed to account for the shifting phenomena that occurs when reducing the demand at a particular time. This factor is still under investigations by the authors and the outcomes will be published in a subsequent paper. The effects of network topology is also studied. It is shown that there is a noticeable difference between a radial and weakly-meshed network in terms of achievable reductions in losses and CVR factor. This fact encourages

a future work to incorporate the network configuration into the VVO framework in order to achieve higher reductions in losses and total demand. Automated switches are required to perform network reconfiguration within DMS capabilities. Further work is to be done for major commercial and industrial customers in terms of CVR factor.

APPENDIX A
POWER FLOW DATA FOR THE 69-NODE SYSTEM

The system power flow data and topology for the 69-node system is provided here, with some modifications, from [20] in Table II. System base voltage is 12.66 kV with $S_{\text{base}} = 1$ MVA. Network topology is reproduced in Fig. 15 for reference.

REFERENCES

[1] I. Roytelman, B. K. Wee, R. L. Lugtu, T. M. Kulas, and T. Brossart, "Pilot project to estimate the centralized volt/VAR control effectiveness," *IEEE Trans. Power Syst.*, vol. 13, no. 3, pp. 864–869, Aug. 1998.

[2] A. Dwyer, R. E. Nielsen, J. Stangl, and N. S. Markushevich, "Load to voltage dependency tests at BC Hydro," *IEEE Trans. Power Syst.*, vol. 10, no. 2, pp. 709–715, May 1995.

[3] V. Dabic, C. Siew, J. Peralta, and D. Acebedo, "BC Hydro's experience on voltage VAR optimization in distribution system," in *IEEE PES T&D*, 2010, pp. 1–7.

[4] N. Markushevich and W. Luan, "Achieving greater VVO benefits through AMI implementation," in *IEEE PES GM*, 2011, pp. 1–7.

[5] R. H. Liang, Y. K. Chen, and Y. T. Chen, "Volt/VAR control in a distribution system by a fuzzy optimization approach," *Int. J. Elect. Power & Energy Syst.*, vol. 33, no. 2, pp. 278–287, 2011.

[6] K. Schneider and T. Weaver, "Volt-VAR optimization on American Electric Power feeders in Northeast Columbus," in *IEEE PES T&D*, 2012, pp. 1–8.

[7] I. Roytelman, B. K. Wee, and R. L. Lugtu, "Volt/VAR control algorithm for modern distribution management system," *IEEE Trans. Power Syst.*, vol. 10, no. 3, pp. 1454–1460, Aug. 1995.

[8] M. E. Baran and M. Y. Hsu, "Volt/VAR control at distribution substations," *IEEE Trans. Power Syst.*, vol. 14, no. 1, pp. 312–318, Feb. 1999.

[9] Y. Liu, P. Zhang, and X. Qiu, "Optimal volt/VAR control in distribution systems," *Int. J. Elect. Power & Energy Syst.*, vol. 24, no. 4, pp. 271–276, 2002.

[10] G. Ramakrishna and N. D. Rao, "Adaptive neuro-fuzzy inference system for volt/VAR control in distribution systems," *Elect. Power Syst. Res.*, vol. 49, no. 2, pp. 87–97, 1999.

[11] B. A. de Souza and A. M. F. de Almeida, "Multiobjective optimization and fuzzy logic applied to planning of the volt/VAR problem in distributions systems," *IEEE Trans. Power Syst.*, vol. 25, no. 3, pp. 1274–1281, Aug. 2010.

[12] B. Milosevic and M. Begovic, "Capacitor placement for conservative voltage reduction on distribution feeders," *IEEE Trans. Power Del.*, vol. 19, no. 3, pp. 1360–1367, Jul. 2004.

[13] K. P. Schneider, F. K. Tuffner, J. C. Fuller, and R. Singh, "Evaluation of conservation voltage reduction (CVR) on a national level," US Department of Energy, Tech. Rep., Jul. 2010.

[14] M. Dong, P. C. M. Meira, W. Xu, and W. Freitas, "An event window based load monitoring technique for smart meters," *IEEE Trans. Smart Grid*, vol. 3, no. 2, pp. 787–796, Jun. 2012.

[15] M.-S. Chen, R. R. Shoults, and J. Fitzer, "Effects of reduced voltage on the operation and efficiency of electric loads," EPRI, Tech. Rep., Sep. 1981.

[16] J. R. Marti, H. Ahmadi, and L. Bashualdo, "Linear power flow formulation based on a voltage-dependent load model," *IEEE Trans. Power Del.*, vol. 28, no. 3, pp. 1682–1690, Jul. 2013.

[17] L. M. Hajagos and B. Danai, "Laboratory measurements and models of modern loads and their effect on voltage stability studies," *IEEE Trans. Power Syst.*, vol. 13, no. 2, pp. 584–592, May 1998.

[18] H. Ahmadi, B. Asaei, and S. Mohseni, "Experimental performance analysis of electronic and magnetic ballasts for fluorescent lamps," in *26th Int. Power Syst. Conf.*, 2012, pp. 1–6.

[19] J. C. Das, *Power System Analysis: Short-circuit Load Flow and Harmonics*. CRC Press, Apr. 2002.

[20] J. S. Savier and D. Das, "Impact of network reconfiguration on loss allocation of radial distribution systems," *IEEE Trans. Power Del.*, vol. 22, no. 4, pp. 2473–2480, Oct. 2007.

[21] *IBM ILOG CPLEX Optimization Studio CPLEX User's Manual*, 12th ed., IBM, 2011.

Hamed Ahmadi received the B.Sc. and M.Sc. degrees in electrical engineering from the University of Tehran in 2009 and 2011, respectively, and is currently a Ph.D. candidate in electrical power engineering at the University of British Columbia, Vancouver, BC, Canada. His research interests include distribution systems analysis, optimization algorithms, power system stability and control, smart grids and high voltage engineering.

José R. Martí (M'80-SM'01-F'02) received the Electrical Engineering degree from Central University of Venezuela, Caracas, in 1971, the Master of Engineering degree in electric power (M.E.E.P.E.) from Rensselaer Polytechnic Institute, Troy, NY, in 1974, and the Ph.D. degree in electrical engineering from the University of British Columbia, Vancouver, BC, Canada in 1981. He is known for his contributions to the modeling of fast transients in large power networks, including component models and solution techniques. Particular emphasis in recent years has been the development of distributed computational solutions for real-time simulation of large systems and integrated multisystem solutions. He is a Professor of electrical and computer engineering at the University of British Columbia and a Registered Professional Engineer in the Province of British Columbia, Canada.

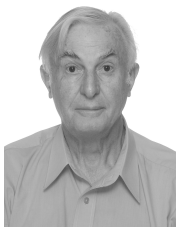

Hermann W. Dommel (LF'01) was born in Germany in 1933. He received the Dipl.-Ing. and Dr.-Ing. degrees in electrical engineering from the Technical University Munich, Munich, Germany, in 1959 and 1962, respectively. From 1959 to 1966, he was with the Technical University Munich, and from 1966 to 1973, he was with Bonneville Power Administration, Portland, OR. Since 1973, he has been with the University of British Columbia in Vancouver, Canada, where he is now Professor Emeritus. He is a Life Fellow of IEEE, and is best known for his work on electromagnetic transients in power systems. In 2013, he was awarded the IEEE Medal in Power Engineering.

Table II
POWER FLOW DATA FOR THE 69-NODE SYSTEM

From	To	$R(\Omega)$	$X(\Omega)$	P (kW)	Q (kVAR)	From	To	$R(\Omega)$	$X(\Omega)$	P (kW)	Q (kVAR)
1	2	0.0005	0.0012	80	45	3	36	0.0044	0.0108	26	19
2	3	0.0005	0.0012	80	45	36	37	0.0640	0.1565	26	19
3	4	0.0015	0.0036	80	45	37	38	0.1053	0.1230	80	45
4	5	0.0251	0.0294	80	45	38	39	0.0304	0.0355	24	17
5	6	0.3660	0.1864	26	22	39	40	0.0018	0.0021	24	17
6	7	0.0801	1.6028	40	30	40	41	0.7283	0.8509	12	10
7	8	0.0922	0.0470	75	54	41	42	0.3100	0.3623	80	45
8	9	0.0493	0.0251	30	22	42	43	0.0410	0.0478	60	43
9	10	0.8190	0.2707	28	19	43	44	0.0092	0.0116	80	45
10	11	0.1872	0.0619	145	104	44	45	0.1089	0.1373	39	26
11	12	0.7114	0.2351	145	104	45	46	0.0009	0.0012	39	26
12	13	1.0300	0.3400	80	50	4	47	0.0034	0.0084	80	45
13	14	1.0440	0.3450	80	55	47	48	0.0851	0.2083	79	56
14	15	1.0580	0.3496	80	45	48	49	0.2898	0.7091	385	275
15	16	0.1966	0.0650	46	30	49	50	0.0822	0.2011	385	275
16	17	0.3744	0.1238	60	35	8	51	0.0928	0.0473	41	28
17	18	0.0047	0.0016	60	35	51	52	0.3319	0.1114	36	27
18	19	0.3276	0.1083	80	45	9	53	0.1740	0.0886	44	35
19	20	0.2106	0.0690	10	6	53	54	0.2030	0.1034	26	19
20	21	0.3416	0.1129	114	81	54	55	0.2842	0.1447	24	17
21	22	0.0140	0.0046	53	35	55	56	0.2813	0.1433	80	45
22	23	0.1591	0.0526	80	45	56	57	1.5900	0.5337	80	45
23	24	0.3463	0.1145	28	20	57	58	0.7837	0.2630	80	45
24	25	0.7488	0.2475	80	45	58	59	0.3042	0.1006	100	72
25	26	0.3089	0.1021	14	100	59	60	0.3861	0.1172	80	45
26	27	0.1732	0.0572	14	100	60	61	0.5075	0.2585	622	444
3	28	0.0044	0.0108	26	19	61	62	0.0974	0.0496	32	23
28	29	0.0640	0.1565	26	19	62	63	0.1450	0.0738	80	45
29	30	0.3978	0.1315	80	45	63	64	0.7105	0.3619	227	162
30	31	0.0702	0.0232	80	45	64	65	1.0410	0.5302	59	42
31	32	0.3510	0.1160	80	45	11	66	0.2012	0.0611	18	13
32	33	0.8390	0.2816	14	100	66	67	0.0047	0.0014	18	13
33	34	1.7080	0.5646	20	14	12	68	0.7394	0.2444	28	20
34	35	1.4740	0.4873	60	40	68	69	0.0047	0.0016	28	20

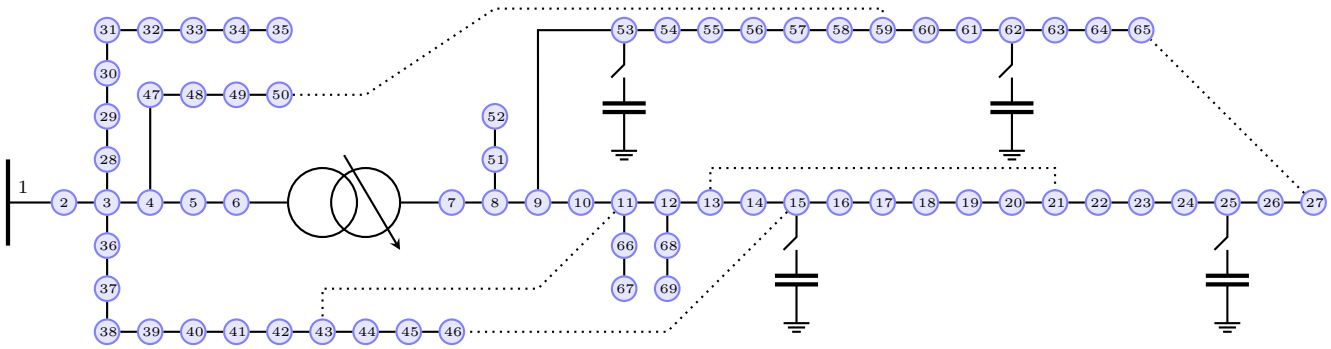

Figure 15. The 69-node system [20]. Dotted lines indicate normally-open switches.